This is a preprint, the final version is subject to change, of the American Mineralogist (MSA)
Cite as Authors (Year) Title. American Mineralogist, in press.
(DOI will not work until issue is live.) DOI: http://dx.doi.org/10.2138/am.2014.4508

Revision 2

X-ray absorption characterization of Cr in forsterite within the MacAlpine Hills 88136 EL3 chondritic meteorite

David A. McKeown[1,*], Andrew C. Buechele[1], Ryan Tappero[2], Timothy J. McCoy[3], and Kathryn G. Gardner-Vandy[3]

[1] Vitreous State Laboratory, The Catholic University of America,

620 Michigan Ave, N.E., Washington, D.C. 20064

[2] 2 Photon Sciences Department, Brookhaven National Laboratory, Upton, NY 11793

[3] Department of Mineral Sciences, National Museum of Natural History,

Smithsonian Institution, Washington, DC 20560-0119

* corresponding author:

Phone: (202) 319-5226, FAX: (202) 319-4469; e-mail: davidm@vsl.cua.edu

Abstract

Chromium K-edge X-ray absorption spectra were collected to characterize Cr in forsterite (Mg_2SiO_4) as well as sulfides within the MAC 88136 EL3 chondrite to determine

Cr valence and to see whether forsterite within this meteorite can be used as a Cr^{2+}-silicate standard. Spectra were measured on several areas within a nearly pure 100 x 200 μm forsterite grain containing 0.13 wt.% Cr. XANES findings indicate highly reduced Cr^{2+} species, with no clear evidence of Cr^{3+} or Cr^{6+}. EXAFS data indicate an average 2.02 Å Cr-O nearest-neighbor distance, consistent with Cr-O distances found in square-planar $Cr^{2+}O_4$ sites observed in synthetic crystalline silicates, and an average 2.69 Å Cr-Si second-nearest neighbor distance, consistent with Cr^{2+} substituting for Mg^{2+} in the forsterite M(1) site. Nearest-neighbor Debye-Waller factor and coordination number parameters indicate Cr^{2+} is likely entering forsterite in disordered sites that are possible intermediates between M(1) and square-planar $Cr^{2+}O_4$ configurations. Preliminary Cr XAS measurements on sulfides within this meteorite also indicate Cr^{2+} in CrS_6 octahedra.

Keywords: Cr^{2+}-silicate, meteorite, X-ray absorption spectroscopy.

This is a preprint, the final version is subject to change, of the American Mineralogist (MSA)
Cite as Authors (Year) Title. American Mineralogist, in press.
(DOI will not work until issue is live.) DOI: http://dx.doi.org/10.2138/am.2014.4508

Introduction

Olivines ($(Mg,Fe)_2SiO_4$) within chondrules in chondritic meteorites sometimes contain significant amounts of chromium (Cr) incorporated into the silicate structure upon crystallization from the molten chondrule. Cr concentrations in unmetamorphosed chondrules can range upward to 1 wt.% Cr_2O_3 (Weisberg et al. (2005)). During subsequent thermal metamorphism, Cr diffuses from the olivine, providing a sensitive indicator of the relative degree of metamorphism (Weisberg et al. (2006); Grossman (2004); Weisberg et al. (2005)). Consequently, olivine within most metamorphosed, chondritic meteorites typically has only trace amounts of Cr. Among those chondritic meteorites with Cr-bearing olivines, those with the most Cr in olivine are the least metamorphosed, including the CO3.0 chondrite Allan Hills (ALH) A77307, the LL3.0 chondrite Semarkona, and the EL3 chondrite MacAlpine Hills (MAC) 88136. MAC 88136 contains forsterite (Mg_2SiO_4) with relatively "high" Cr-concentrations of up to 0.7 wt.% Cr_2O_3 (Weisberg et al. (1994); Weisberg et al. (2005)).

The initial interest in characterizing chondritic Cr-bearing olivines is to identify a crystalline Cr^{2+}-silicate standard to use for Cr valence X-ray absorption spectroscopy (XAS) studies of silicates synthesized under reducing conditions (McKeown et al. (2011)). At the same time, understanding Cr valence states sheds light on the fO_2 conditions of formation of these meteorites. Cr^{2+} silicates are not readily found in the oxidizing environments at or near the Earth's crust, where Cr species are typically 6+ or 3+. In contrast, chondrule formation, crystallization, and chondrite metamorphism likely occurred under relatively

reducing conditions, with fO_2 ranging from ~IW (iron-wustite) to ~IW-8 (Fogel et al., 1989). Previous work has demonstrated the predominance of Cr^{2+} among chondrule olivines (Sutton et al. (1996)), with the FeO-rich olivines in the CO3.0 chondrite ALH A77307 having a lower Cr^{2+}/Cr^{3+} ratio (~0.3) than the FeO-poor olivines in the LL3.0 chondrite Semarkona (~0.9) (Sutton et al. (1996)). Extending this trend, we have studied the relatively Cr-rich and FeO-poor olivines from the highly-reduced EL3 chondrite MAC 88136 to improve the chances of collecting better signal-to-noise Cr^{2+}-silicate XAS data.

An X-ray absorption spectrum is divided into two regions: the X-ray absorption near edge structure (XANES) that includes an absorption edge of the element of interest, and the extended X-ray absorption fine structure (EXAFS). The slope and shape of the absorption edge rise as well as the overall edge energy are sensitive to the valence of the absorbing element, where the overall edge energy increases with higher (more oxidized) valences. Relatively narrow features at the absorption edge can be due to single and multiple scattering contributions from the local atomic environment surrounding the absorbing element. The EXAFS data, by convention, are extracted from a spectrum at approximately 20 eV beyond the absorption edge to higher energies. In many cases, EXAFS oscillations are due primarily to single scattering of the spherical electron wave emitted by the absorbing atom (in this case Cr) from the arrangement of atoms surrounding the absorber. Through fitting procedures, EXAFS data are analyzed to quantitatively determine average bond distance (r (Å)), coordination number (n (atoms)), and disorder or Debye-Waller factor (σ^2 ($Å^2$)) of shells of atoms around the absorber.

This is a preprint, the final version is subject to change, of the American Mineralogist (MSA)
Cite as Authors (Year) Title. American Mineralogist, in press.
(DOI will not work until issue is live.) DOI: http://dx.doi.org/10.2138/am.2014.4508

Comparisons of the Cr XANES data for Cr-olivine in MAC 88136 with that for Cr^{3+} in uvarovite ($Ca_3Cr_2Si_3O_{12}$), Cr^{6+} in crocoite ($PbCrO_4$), and Cr^0 in Cr-foil crystalline standards, will determine whether the Cr is reduced to 2+. Any Cr EXAFS findings for these olivines will be compared with Cr-O distances in $Cr^{2+}O_4$ sites determined in synthetic crystalline silicates (Dollase, et al. (1994); Miletich, et al. (1997)). Due to ionic radii considerations, Cr^{2+} within olivine should substitute for Mg^{2+} in the octahedral M-sites (Boström (1987)); therefore, the EXAFS findings may be able to verify this type of site substitution for Cr in the forsterite structure.

Earlier Cr XANES studies observed Cr^{2+} in lunar and terrestrial silicate glasses and crystals (Sutton et al. (1993); Goodrich et al. (2012); Berry et al., (2006); Berry, A.J. and O'Neill (2004)). Comparisons of Cr XANES spectra for synthetic Cr-doped forsterites and borosilicate glasses with Cr having predominantly 2+ and 3+ valences show an energy shift in the edge from 3 to 5 eV between these two valences (Fig. 2 in Sutton et al. (1993)). In the same study, XANES data from a lunar mare basalt sample also indicated Cr^{2+} in olivine with Cr^{3+} in pyroxene, probably indicating preferential incorporation of specific Cr valence species into different mineral structure types (Sutton et al. (1993)). Cr XANES studies have also been done on composition and redox effects in silicate glasses, and show a similar progressive shift to lower edge energies where oxygen fugacities are varied from $\log fO_2 = 0$ to -16 at 1400 ºC (Berry et al., (2006); Berry and O'Neill (2004)); these findings relied on

$Cr^{2+}/Cr_{(total)}$ results using a standardless analysis routine, where intensity changes in a XANES derivative feature near 5994 eV varied linearly with the theoretical dependence of $\log fO_2$ for the glass systems investigated. Interestingly, these experiments showed a shift in $Cr^{2+}/ Cr_{(total)}$ from ~0.7 at ~IW ($\log fO_2 = -9$ at 1400°C) to ~1 at ~IW-6 ($\log fO_2 = -16$ at 1400°C). A recent study of ureilite achondritic meteorites (Goodrich et al. (2012)) presented preliminary findings for Cr valence in olivines that showed a trend of Cr valence decreasing as olivine compositions approach forsterite. In these studies, the Cr findings cannot verify if 100% of all Cr is Cr^{2+} within of the samples measured. Results from the above studies will be compared with the XANES findings determined here for Cr-olivine within MAC 88136.

Experimental

Cr K-edge XAS data are typically used to characterize bulk Cr valence and coordination environments in silicates over Cr L-edges for a number of practical reasons. In the case of this study, it was possible to gather XAS data only at the Cr K-edge, due to restrictions of the energy range available on the beam line used.

Cr K-edge XAS were measured for two crystalline standards, uvarovite (NMNH #106331 from Finland) that contains $Cr^{3+}O_6$ octahedra (Novak and Gibbs (1971)), and crocoite (NMNH #157582 from Australia) that contains $Cr^{6+}O_4$ tetrahedra (Quareni and De Pieri (1965)). These standards were ground and sieved to powders with particle diameters

This is a preprint, the final version is subject to change, of the American Mineralogist (MSA)
Cite as Authors (Year) Title. American Mineralogist, in press.
(DOI will not work until issue is live.) DOI: http://dx.doi.org/10.2138/am.2014.4508

near one absorption length for Cr at the Cr K-edge energy. Phase identification of these samples was verified by powder X-ray diffraction.

A polished thin-section (30 μm thickness) of MAC 88136,47 was obtained (from NASA Johnson Space Center) so that the mineral grains could be readily identified using optical crystallography, micro-Raman spectroscopy, and scanning electron microscopy – energy dispersive spectroscopy (SEM-EDS) techniques. Olivine is typically a minor mineral component (approximately 2 to 7 volume %) within unequilibrated enstatite chondrites (Weisberg et al. (2005)), where mineral grains are usually 10's μm in diameter. Several forsterite grains were found in this sample, where the largest grain is approximately 200 x 100 μm occurring within an ~1 mm diameter porphyritic olivine pyroxene chondrule (Fig. 1). Identification of the forsterite grains in the thin-section was accomplished using a Nikon SMZ1500 binocular microscope, where forsterite grains can be clearly distinguished from surrounding enstatite ($Mg_2Si_2O_6$), metal, and sulfide phases by their transparency and high-order birefringent colors under transmitted cross-polarized light (Fig. 1) (Heinrich (1965)). Phase characterization of the largest forsterite grain found in this thin-section was verified by Raman spectroscopy as well as chemical analyses from scanning electron microscopy - energy dispersive analysis (SEM-EDS). Raman spectra of the olivine grains indicate forsterite, where ten of the strongest Raman modes from these grains are observed to be within 2 cm^{-1} of the more prominent peaks measured for synthetic forsterite (McKeown et al. (2010); the Raman spectra for this Cr-forsterite are averages of the oriented single crystal spectra, which indicate that this forsterite grain is polycrystalline down to the 10 μm diameter scale of the incident laser beam.

This is a preprint, the final version is subject to change, of the American Mineralogist (MSA)
Cite as Authors (Year) Title. American Mineralogist, in press.
(DOI will not work until issue is live.) DOI: http://dx.doi.org/10.2138/am.2014.4508

The Cr-containing forsterite grain measured had its composition determined by SEM-EDS (Table 1) on several analysis areas. The thin section was first coated with 150 nm of carbon in a vacuum evaporator and adhered to an aluminum stub using conductive tape linked to the carbon coating establishing a conductive path to prevent charging in the SEM. The instrument used was a JEOL JSM 5910-LV SEM operating at 20 kV accelerating potential and equipped with an Oxford INCA Energy 300 X-ray analysis system. A beam current of 5 nA was used to enable rapid acquisition of spectra with sufficient total count statistics to measure the low levels of Cr present in the forsterite grain. Process time was selected to maintain a deadtime of 30-40%. The grain was located using surface features visible in the light-optical micrograph (Fig. 1) of the specimen taken before it was placed in the SEM. Imaging of the thin section was done in the electron backscatter mode which clearly revealed tiny sulfide or spinel inclusions in the grain which were avoided in selecting spots to place the electron beam for spectrum collection. Spectra were collected at three separate locations on the grain: two for 15 seconds live time, each containing about 3.5 x 10^5 total counts, and one for 60 seconds live time containing about 1.4 x 10^6 total counts. The spectra were processed using the INCA software to produce the quantitative results for Mg, Si, Cr, Mn, and Fe. Oxygen was determined by stoichiometry, and Fe was assumed to be in the 2+ state. SEM-EDS analyses indicate weight percentages of Mg, Si, and oxygen that are close to ideal values for forsterite (Mg_2SiO_4) (Table 1) with minor amounts of Cr (0.13 wt.%) and Fe (0.36 wt.%) and traces of Mn in one analysis. The composition of this grain can be expressed as $Fo_{99.5}$ from the Mg/(Mg+Fe) ratio.

This is a preprint, the final version is subject to change, of the American Mineralogist (MSA)
Cite as Authors (Year) Title. American Mineralogist, in press.
(DOI will not work until issue is live.) DOI: http://dx.doi.org/10.2138/am.2014.4508

To obtain XAS spectra specific to these small grains, data were collected at the μ-XAS Beam Line X27-A at the NSLS, where the incident beam was focused to a 14 x 7 μm area on the sample. The XAS data were collected under synchrotron running conditions near 250 mA and 2.8 GeV. The X27-A monochromator consisted of two water-cooled Si(111) channel-cut crystals, with a four-jaw motorized slit system located immediately upstream of this arrangement. The energy resolution for the XAS spectra at the Cr K-edge is near 1 eV. The micro-focusing of the incident X-ray beam was done by using two, 20 cm long, dynamically bent rhodium-coated silicon mirrors arranged in Kirkpatrick-Baez (KB) geometry, which is housed within a helium-purged enclosure. The KB mirrors focused the incident beam to a 7 x 14 μm spot on the sample. Fluorescence spectra were gathered using a Canberra 13-element Germanium Array X-ray detector to measure the fluorescence X-ray intensity (I_f) from the sample and an ion chamber to measure the incident beam intensity (I_0). XAS data were collected from 5860 to 6480 eV, that included the Cr K-absorption edge near 5989 eV. Each XAS spectrum collected is the absorption coefficient (μ) of the sample versus energy, where μ is proportional to I_f / I_0. A Cr foil (Cr^0) was measured to energy-calibrate the XAS data gathered for the samples. XAS data for the Cr-forsterite grain were collected at or near the areas that were measured by SEM-EDS and Raman spectroscopy.

This is a preprint, the final version is subject to change, of the American Mineralogist (MSA)
Cite as Authors (Year) Title. American Mineralogist, in press.
(DOI will not work until issue is live.) DOI: http://dx.doi.org/10.2138/am.2014.4508

Data Analysis

Fluorescence XAS data were collected, where at least two spectra were collected for each point on each sample and were averaged together for analysis. The XANES spectra presented were initially processed using standard pre-edge background subtraction and edge-step normalization procedures (Sayers and Bunker (1988)). The derivative maximum of the Cr K-absorption edge for Cr foil was calibrated to 5989 eV (Fig. 2) and defined to be E_0 to energy-calibrate the Cr K-absorption edge in all XAS spectra for all samples measured. After normalization and calibration, direct comparisons can be made with the XANES data for all samples to an energy accuracy of $\pm$ 0.3 eV, or the energy difference between two adjacent data points at the edge (Fig. 2). Any XANES fitting, to determine Cr valence populations in this study, was done using the linear combination fitting routine in the analysis software Athena in iXAS. (Newville (2001); Ravel and Newville (2005)). A cubic spline function was fit to and then subtracted from the edge-step normalized EXAFS data from 10 to 500 eV above E_0. Energy values in eV were converted to k ($Å^{-1}$) (Sayers and Bunker (1988)), where the resulting $\chi(k)$ data was k^2-weighted (Fig. 3a). The $k^2\chi(k)$ data were then Fourier-transformed over the $2.2 \leq k \leq 10.4$ $Å^{-1}$ range. A Hanning window of 1.0 $Å^{-1}$ was used on the upper and lower limits of the $k^2\chi(k)$ data to minimize Fourier-transform termination artifacts in the resulting partial radial distribution function (RDF). Peaks in the RDFs correspond to shells of atoms surrounding Cr (Fig. 3b), where r, n, and σ^2 for each atomic shell can be obtained from the fitting procedure in the EXAFS analysis software

Artemis in iXAS (Newville (2001); Ravel and Newville (2005)). The position of each peak in the RDF is phase-shifted to lower r by approximately 0.3 to 0.5 Å with respect to the actual bond distance that corresponds to each peak. The RDF fitting range for the crocoite and uvarovite standards was from 0.8 to 1.9 Å and from 1.0 to 3.4 Å, respectively, using a Hanning window of 0.5 Å. The RDF fitting range for the Cr-forsterite data was from 0.7 to 5.4 Å, using the same Hanning window as the standards, that included the two nearest-neighbor peaks near 1.5 and 2.2 Å , as well as the broad features from 3.0 to 5.5 Å (Fig. 3b).

Atom clusters, surrounding a central Cr atom to a maximum radial distance of 6 Å, were generated to simulate the crystal structures for crocoite (Quareni and De Pieri (1965)), uvarovite (Novak and Gibbs (1971)), and forsterite (Boström (1987)) (two clusters with Cr in each of the M(1) and M(2) sites). These clusters were used by FEFF7.02 (Newville (2001); Ravel and Newville (2005)) to calculate the theoretical EXAFS for each sample. By taking into account the important atom correlations calculated by FEFF from the atom clusters, Cr-O, Cr-Ca, and Cr-Si path contributions could then be used to label the RDF peaks for uvarovite (Fig. 3b). Uvarovite was the standard used as the basis of the first-shell RDF peak fitting for the Cr-forsterite EXAFS data. The dominant contributions to the theoretical X-ray absorption spectrum for uvarovite are the six Cr-O nearest-neighbor single scattering paths at 1.98 Å (Novak and Gibbs (1971)).

This is a preprint, the final version is subject to change, of the American Mineralogist (MSA)
Cite as Authors (Year) Title. American Mineralogist, in press.
(DOI will not work until issue is live.) DOI: http://dx.doi.org/10.2138/am.2014.4508

Discussion

Cr XANES

The Cr K-edge spectra for the standards (Fig. 2) show a systematic shift to higher energy of the main edge as the Cr valence increases from 0 (Cr-foil) to 3+ (uvarovite) to 6+ (crocoite), similar to spectra presented earlier (Berry and O'Neill (2004); Berry et al. (2006); McKeown et al. (2011)). The Cr XANES spectrum for Cr-forsterite (Fig. 2, blue points and line) indicates that the Cr K-edge is at lower energies than that for Cr^{3+} in uvarovite, basically reproducing trends seen earlier for Cr^{2+} in silicate glasses and lunar basalts (Sutton et al. (1993). These data show that the Cr valence in Cr-forsterite is clearly more reduced than Cr^{3+} in uvarovite, and is at least dominated by Cr^{2+}.

Cr EXAFS Data and Analysis

The $k^2\chi(k)$, partial RDF, and EXAFS analysis results for the standards uvarovite and crocoite are similar to those results presented earlier (McKeown et al. 2011)(Table 2; Figs. 3a and b: only uvarovite data are presented). The uvarovite was selected for comparison with Cr-forsterite (Figs. 3a and b), since Cr^{2+} in forsterite would most likely be in the M-octahedral sites, or configurations more like the octahedral Cr^{3+} site in uvarovite than the

tetrahedral Cr^{6+} environment in crocoite. The $k^2\chi(k)$ and partial RDF data for Cr-forsterite show significant differences with respect to the equivalent data for uvarovite. EXAFS oscillations for Cr-forsterite have roughly the same periodicity as that observed for uvarovite, indicating similar Cr-O distances; but, oscillation amplitudes for Cr-forsterite are significantly smaller compared with those for uvarovite (Fig. 3a).

Cr-forsterite EXAFS fitting results (Table 3; Fig. 4) that best describe the two main peaks in the partial RDF include Cr-O for the 1.5 Å peak, and Cr-Si for the 2.2 Å peak. The Cr-O nearest-neighbor distance of 2.02 Å, slightly longer than that in uvarovite (1.98 Å), is within the range of Cr-O distances found in square-planar $Cr^{2+}O_4$ environments (Fig. 5) in crystalline silicates such as Cr_2SiO_4 (Dollase et al. (1994)) and $XCrSi_4O_{10}$ gillespite-type structures (where: X = Ca,Ba,Sr)(Miletich et al. (1997)). Both *n* and σ^2 determined for Cr-forsterite indicate reduction in EXAFS amplitude with respect to uvarovite (Tables 2 and 3). The small 2.6 coordination number and large 0.0037 $Å^2$ Debye-Waller factor likely indicate a significantly wider range of nearest-neighbor Cr-O distances around Cr in forsterite than what is found in the octahedral Cr-site in uvarovite, where all six Cr-O distances are the same. The second-nearest neighbor Cr-Si *r* and *n* parameters (2.69 Å and 1.8, respectively) indicate that Cr is more likely entering the M(1) site in the forsterite structure than M(2), which has a Cr-Si distance of 2.79 Å with a coordination of 1.0 (Table 3). Cr entering the M(1) site also makes sense in light of Mg-O distances in M(1) and M(2) in forsterite (Fig. 5); Mg-O distances in M(1) range from 2.07 to 2.13 Å and are closer to the 2.02 Å Cr-O distance for Cr-forsterite, than the longer 2.05 Å to 2.22 Å Mg-O distances in M(2).

This is a preprint, the final version is subject to change, of the American Mineralogist (MSA)
Cite as Authors (Year) Title. American Mineralogist, in press.
(DOI will not work until issue is live.) DOI: http://dx.doi.org/10.2138/am.2014.4508

To provide a better fit to the overall $k^2\chi(k)$ data and partial RDF for the meteorite, two more distant correlations were used to fit the broad series of RDF features from 3.5 to 5.6 Å (Fig. 4) that are caused by many overlapping contributions in the crystal structure around Cr. There are 38 Cr-O, 8 Cr-Si, and 16 Cr-Mg pair correlations in the forsterite structure up to 6 Å around the M(1) site. The two additional paths used for the fitting resulted in 7 x Cr-O at 4.60 Å and 6 x Cr-Mg at 5.68 Å, which correspond to actual Cr-O and Cr-Mg correlations at those distances in the atom distribution around a Cr-containing M(1) site.

The fitting parameters from the EXAFS analysis indicate that the average nearest-neighbor Cr environment in forsterite can be interpreted as a disordered version of a square-planar $Cr^{2+}O_4$-site. This disorder can produce a larger σ^2 compared with the two standards (Tables 2 and 3), but can also reduce *n* to 2.6, from the expected 4.0 for square planar sites. This small nearest-neighbor coordination number also indicates that significant populations of six-fold Cr^{3+} environments in this forstetite grain are unlikely. Large site disorder can produce low coordination numbers from EXAFS analysis, because the technique may not sense all atoms in a non-Gaussian distribution around the absorbing atom (Eisenberger and Brown (1979)). EXAFS data and analysis results for Cr-forsterite indicate a significantly different Cr environment from the CrO_6 octahedra in uvarovite as well as from the MgO_6 M(1) environment in forsterite (Fig. 5).

Cr^{2+} in forsterite appears to distort the original nearest-neighbor configuration of the M(1) site to conform somewhat to a square-planar environment. The octahedral M(1) site in forsterite has an average Mg-O distance of 2.10 Å, which is longer than the average 2.02 Å Cr-O distance determined for Cr in forsterite by EXAFS (Table 3). The EXAFS fitting results indicate that the average environment around Cr in forsterite can be a disordered intermediate between CrO_4 square-planar and M(1) octahedral sites. The contrast of the EXAFS determined Cr environment in forsterite with respect to the M(1) configuration (Fig. 5) may indicate that Cr entering the M(1) sites may cause disorder – distortion within those sites.

Cr-Forsterite as a Cr^{2+} Standard

An objective for measuring Cr XAS of Cr-forsterite in meteorite MAC88136 is to verify that this sample can be used as a Cr^{2+} standard data for characterizing reduced Cr in other silicates. XANES data and analysis results indicate that Cr^{2+} is the dominant valence in this grain. The EXAFS determined nearest-neighbor Cr-O distance, coordination number, and Debye-Waller factor are consistent with disorderd $Cr^{2+}O_4$ square planar environments, where significant populations of octahedral $Cr^{3+}O_6$ are unlikely in this grain. How certain that 100% of all Cr in the forsterite grain measured is Cr^{2+}, is hard to determine solely from the XAS data and findings presented above.

One approach to address this issue can be found from arguments in the meteorite literature. Preliminary Cr XAS studies of olivine within ureilite meteorites (Goodrich et al. (2012)) suggest that average Cr valence decreases from 2.4 and 2.1 as olivine compositions become more Mg-rich from Fo_{74} to Fo_{92}. By considering this composition versus Cr valence relationship and the $Fo_{99.5}$ composition olivine measured in MAC 88136, the Cr valence in this olivine grain is likely to be more reduced than 2.1, or approaching 2.0 and 100% Cr^{2+}. Comparison between enstatite chondrites and ureilites is justified, given that the olivine in enstatite chondrites occurs within the once-molten chondrules and the olivine in ureilites – which are primitive achondrites that experienced low degrees of partial melting – is a residual phase that formed originally within chondrules, not as a crystallization product from the melting that occurred during urelite formation. These findings are also consistent with approximate inferred liquidus temperatures and oxygen fugacities for chondrule formation in enstatite chondrites within the range of the 1400°C, log fO_2 = -16 experiments of Berry et al. (2006) that produced ~100% Cr^{2+}.

Another approach to address this issue was done by additional Cr XAS measurements on well characterized redox Cr-silicate glasses studied in Schreiber and Hockman (1987). Cr XANES spectra were subsequently measured on four silicate glasses synthesized under different redox conditions, where XANES data from the Cr-forsterite in meteorite MAC 88136 (assuming 100% Cr^{2+}) and from the uvarovite standard (having 100% Cr^{3+}) were used to fit these data. The four glasses are from two glass series containing 1 wt% Cr, that were synthesized under a variety of atmospheres where log fO_2

varied from 0 to –14.5. The Cr valence distributions within each glass were originally determined by colorimetry (Schreiber and Hockman (1987)), so that the four glasses measured by XANES have known Cr valence populations ranging from 100% Cr^{3+} to 40% Cr^{3+} + 60% Cr^{2+}. The Cr XANES fitting results for the four glasses are all within ± 6% of those colorimetry-determined values for Cr^{3+} and Cr^{2+} (Table 4 and Fig. 6). Therefore, these XANES findings indicate that reasonable Cr valence distribution results on reduced Cr-silicate glasses can be obtained by using Cr-forsterite as a Cr^{2+} standard. Considering the minor differences in the Cr^{2+}/Cr^{3+} ratio determined from colorimetry versus Cr XANES fitting, a reasonable upper limit for Cr^{3+} is 5% of all Cr in the forsterite measured.

Results from XANES fitting routines using crystalline standards to fit glass data should be viewed with some caution. Linear combinations of the Cr-olivine and uvarovite Cr-edges describe the major Cr XANES features and changes for the reduced Schreiber glasses measured (Fig. 6), as well as provide reasonable estimates of the Cr valence populations in those glasses ((Table 4). However, relatively narrow features in the XANES of the crystalline standards (e.g., edge peak shoulders near 5996 and 6003 eV for Cr-olivine and narrow peaks near 6000, 6007, and 6010 eV for uvarovite (Fig. 2)) are likely caused by single or multiple scattering interference effects from nearest neighbor atoms as well as more distant atom neighbors in the crystal structure surrounding Cr in these standards, that may not be present in the XANES of the structurally disordered glasses. These differences can cause deviations in the best linear combination fit of the standards XANES to the glass

XANES (Fig. 6) and add some uncertainty to the fitting results and interpretations. Using Cr valence glass standards to fit glasses of unknown Cr valence can reduce these uncertainties. This was observed characterizing Tc valence in borosilicate glasses (Lukens et al. 2007), where two well-characterized glass valence standards were used. The Tc K-edge XANES for these two glasses provided better fits to the XANES for glasses with unknown Tc valence distributions, than using crystalline Tc-oxide standards. Unfortunately, a controlled atmosphere furnace necessary to accurately and reproducibly control the Cr valence in silicate melts to produce 100% Cr^{2+}, Cr^{3+}, or Cr^{6+} silicate glasses was not available for this study.

Implications of Cr^{2+} Olivine in Enstatite Chondrites

It is not surprising that enstatite chondrites would be more reduced than any other meteorite for which the Cr valence state has been determined. Formed at exceptionally low oxygen fugacities, we typically find elements that are normally lithophile on Earth behaving as chalcophiles or siderophiles in enstatite chondrites. This behavior produces a broad array of unusual sulfides (e.g., the calcium sulfide oldhamite), metals (e.g., the nickel silicide perryite) and nitrides (e.g., the titanium nitride osbornite). However, the finding of Cr^{2+} in the unequilibrated enstatite chondrite MAC 88136 constrains the formation of this group of meteorites. Weisberg et al. (2011) argued that olivine and FeO-rich pyroxene found in chondrules in unequilibrated enstatite chondrites may have formed under more oxidizing conditions, perhaps in the same oxygen isotopic reservoir. Weisberg et al. (1995) argued on

the basis of modes and compositions primarily of metal and sulfides that EL3 chondrites like MAC 88136 formed under conditions of higher fO_2 than EH3 chondrites. Further, the formation of EL6 chondrites from EL3 chondrites would require reduction of Si^{4+} from the silicates to Si^{0} and incorporation into metal.

While EL3 chondrites may have formed under more oxidizing conditions than either EH3 chondrites or EL6 chondrites, those conditions were still remarkably reducing. Experiments suggest production of 100% Cr^{2+} at oxygen fugacities of ~IW-6 at temperatures comparable to the liquidus of olivine-bearing enstatite chondrite chondrules (Berry et al. (2006)). Our finding of essentially 100% Cr^{2+} in olivine within a MAC 88136 chondrule suggests formation at comparably reducing conditions. If EH3 chondrites were formed at more reducing conditions or metamorphism of EL3 chondrites to form EL6 chondrites requires reduction, those materials formed at conditions more reducing than ~IW-5. Fogel et al. (1989), in fact, suggested metamorphism of the EL6 chondrite Jajh deh Kot Lalu at oxygen fugacities from IW-7 to IW-8 at temperatures of 900-1100°C. Under such conditions, silicon can coexist as Si^{4+} in silicates or Si^{0} in metal and reduction can mobilize silicon between these two phases, as suggested by Weisberg et al. (1995).

This is a preprint, the final version is subject to change, of the American Mineralogist (MSA)
Cite as Authors (Year) Title. American Mineralogist, in press.
(DOI will not work until issue is live.) DOI: http://dx.doi.org/10.2138/am.2014.4508

Cr Sulfides in MAC 88136

The finding of 100% Cr^{2+} in MAC 88136 olivines and suggestions from experiments that all chromium in these highly reduced systems should be in the 2+ valence state has important implications for sulfides that co-exist within enstatite chondrites. Chromium in enstatite chondrites is typically concentrated in sulfides, particularly daubreelite ($FeCr_2S_4$), although it also occurs in brezinaite (Cr_3S_4), heideite ($(Fe,Cr)_{1+x}(Ti,Fe)_2S_4$) and caswellsilverite ($NaCrS_2$). Within these phases, chromium is typically thought to exist in the 3+ valence state, as argued by Okada and Keil (1982) for caswellsilverite and daubreelite, although Keil and Brett (1974) suggested the Cr in heideite occurs in the 2+ valence state. To resolve whether chromium in enstatite chondrite sulfides exists in the 2+ or 3+ state, preliminary Cr XAS spectra were collected on a 10 mm x 5 mm diameter MAC 88136 meteorite fragment (using a 0.7 x 10 mm incident beam on NSLS Beam Line X23-A2) as well as on an opaque grain (using the 7 x 14 μm incident beam on NSLS Beam Line X27-A) in the associated thin section. The XANES spectra (to be shown elsewhere) for both samples are similar and indicative of Cr-sulfides, which is not surprising considering the mineralogy of this meteorite (Lin et al. (1991)). The Cr K-edges for these sulfide spectra are at energies similar to those for Cr^{2+} in forsterite, indicating Cr^{2+} as the dominant species. Cr EXAFS data are also similar for both samples and the resulting analyses indicate S nearest-neighbors with Cr-S distances near 2.39 Å and coordination numbers near 5; these are similar to structural parameters expected for CrS_6 octahedra in brezinaite (Cr_3S_4) (Jellinek, (1957)) and daubreelite ($FeCr_2S_4$) (Raccah et al. (1966)). Unfortunately, the EXAFS determined Cr-

S distances in sulfides cannot be used to discriminate Cr^{2+} from Cr^{3+} to complement the XANES findings, since average Cr-S distance distributions within octahedral environments for these two valences overlap. Further work on chromium valence in chromium-bearing sulfides is warranted to determine whether Cr^{2+} is the dominant valence, with sulfur-sulfur bonds necessary for charge balance, or whether Cr^{3+} is present. At more oxidizing conditions (~IW), the sub-equal mixture of Cr^{2+} and Cr^{3+} partitions between Cr^{3+}-bearing spinel and Cr^{2+}-bearing olivine (Hanson and Jones (1998)).

Concluding Remarks

Chromium K-edge XAS data collected and analyzed for a Cr-forsterite ($Fo_{99.5}$) grain within the unequilibrated EL3 enstatite chondrite meteorite MAC 88136, indicate this grain crystallized under extremely reducing conditions, where disordered $Cr^{2+}O_4$ square-planar environments are probably within the M(1) sites in the forsterite lattice (Fig. 7). Cr XANES of the forsterite grain shows an absorption edge that is shifted to lower energies by approximately 5.3 eV with respect to that for the Cr^{3+} silicate standard, uvarovite, typical of that found for Cr^{2+} in borosilicate glasses as well as synthetic Cr-doped enstatites and forsterites synthesized under highly reducing conditions. To the best of our knowledge, for the first time, EXAFS data were collected and analyzed for a Cr^{2+} environment in a silicate phase, where the first-shell analysis results for the Cr-forsterite grain indicate an average Cr-

O distance near 2.02Å, a small coordination number of 2.6, and a large Debye-Waller factor of 0.0037 $Å^2$, which are consistent with disordered $Cr^{2+}O_4$ square-planar environments. EXAFS analysis of the second nearest-neighbor Cr-Si pair correlations indicate that Cr is likely substituting for Mg in the forsterite M(1) site. This finding is consistent with an earlier model (Burns (1973)) indicating Cr^{2+} would preferentially enter the M(1) sites in olivine inclusions in kimberlite diamonds from the deep upper mantle.

From the XAS findings above, from Cr valence versus olivine composition arguments in the meteorite literature, and from Cr XANES fitting results of four well-characterized redox silicate glasses, it is reasonable to conclude that the valence distribution of Cr in forsterite within meteorite MAC 88136 is near 100% Cr^{2+} with an upper limit of 5% for Cr^{3+}. Therefore, this sample may be useful as a Cr^{2+} silicate XANES standard for the study of reduced Cr valences in silicates, considering the limitations of XANES fitting.

Cr K-edge XANES and EXAFS can be useful to distinguish different Cr valences and associated coordination environments in crystalline and amorphous silicates. The contrast in the XANES and EXAFS data between Cr^{6+} and Cr^{3+} is good to the point that consistent valence percentages can be determined from both types of data (McKeown et al. 2011). However, as shown in this study, the contrast between Cr^{3+} and Cr^{2+} is good only for XANES, and poor for EXAFS. Typical Cr-O nearest neighbor distances and coordination numbers between octahedral $Cr^{3+}O_6$ and square-planar $Cr^{2+}O_4$ environments

are not different enough to quantitatively determine a Cr^{2+}/Cr^{3+} ratio in a sample. However, the structural information obtained from EXAFS should compliment the valence information for sanples containing Cr^{2+} and Cr^{3+}.

Acknowledgments

Portions of this work were performed at Beamline X27-A, National Synchrotron Light Source (NSLS), Brookhaven National Laboratory (BNL). X27-A is supported in part by the U.S. Department of Energy (DOE) - Geosciences (DE-FG02-92ER14244 to The University of Chicago - CARS). Use of the NSLS was supported by DOE, Office of Science, Office of Basic Energy Sciences, under Contract No. DE-AC02-98CH10886. We thank J.E. Post and P. Pohwat (Mineral Sciences Department, National Museum of Natural History, Smithsonian Institution) for supplying the crocoite and uvarovite standards. We also thank Prof. H.D. Schreiber (Virginia Military Institute) for providing the A- and U-series Cr-silicate glasses. We appreciate the assistance of Kevin Righter (NASA Johnson Space Center) and the Meteorite Working Group for supplying a thin section and a bulk fragment of meteorite MAC 88 136. We also thank J.C. Woicik (NIST) and G. Sterbinsky (NIST-NSLS) for their help with data collection on the bulk meteorite sample at NSLS Beam Line X23-A2.

References

Berry, A.J. and O'Neill, H. St.C. (2004) A XANES determination of the oxidation state of chromium in silicate glasses. American Mineralogist, 89, 790-798.

Berry, A.J., O'Neill, H. St.C., Scott, D.R., Foran, G.J., and Shelley, J.M.G. (2006) The effect of composition on Cr^{2+}/Cr^{3+} in silicate melts. American Mineralogist 91, 1901-1908.

Boström, D. (1987) Single-crystal X-ray diffraction studies of synthetic Ni-Mg olivine solid solutions. American Mineralogist, 72, 965–972.

Burns, R.G. (1973) On the Occurrence and Stability of Divalent Chromium in Olivines included in Diamonds. Contributions to Mineralogy and Petrology 51, 213-221.

Dollase, W.A., Seifert, F., O'Neill, H.St.C. (1994) Structure of Cr_2SiO_4 and possible metal-metal interactions in crystal and melt. Physics and Chemistry of Minerals, 21, 104-109.

Eisenberger, P. and Brown, G.S. (1979) The study of disordered systems by EXAFS: Limitations. Solid State Communications, 29, 481–484.

Fogel, R.A., Hess, P.C., and Rutherford, M.J. (1989) Intensive parameters of enstatite chondrite metamorphism. Geochimica et Cosmochimica Acta, 53, 2735-2746.

Goodrich, C.A., Sutton, S.R., and Wirick, S. (2012) Valences of Cr in ureilite olivine and implications for ureilite petrogenesis. Lunar and Planetary Science Conference XXXVI, Abstract No. 1221.

Grossman, J.N. (2004) Loss of chromium from olivine during the metamorphism of chondrites. Lunar and Planetary Science Conference XXXV, abstract 1320.

Hanson B. and Jones J.H. (1998) The systematics of Cr^{3+} and Cr^{2+} partitioning between olivine and liquid in the presence of spinel. American Mineralogist 83, 669-684.

Heinrich, E.W. (1965) Microscopic Identification of Minerals" (McGraw-Hill, Inc., New York), p. 144, 200.

Jellinek, F. (1957) The structures of the chromium sulphides. Acta Crystallographica 10, 620-628.

Keil, K. and R. Brett (1974) Heideite, $(Fe, Cr)_{1+x}(Ti, Fe)_2S_4$, a new mineral in the Bustee enstatite achondrite. American Mineralogist, 59, 465–470

Lin, Y.T., Nagel, H.-J., Lundberg, L.L., El Goresy, A. (1991) MAC88136 – the first EL3 Chondrite. Lunar and Planetary Science Conference XXII, 811-812.

Lukens, W.W., McKeown, D. A., Buechele, A. C. , Muller, I. S. , Shuh, D. K., and Pegg I. L. (2007) Dissimilar Behavior of Technetium and Rhenium in Borosilicate Waste Glass as Determined by X-ray Absorption Spectroscopy. Chemistry of Materials, 19, 559-566.

McKeown, D.A., Bell, M.I., and Caracas, R. (2010) Theoretical Determination of the Raman Spectra of Single Crystal Forsterite (Mg_2SiO_4). American Mineralogist, 95, 980-986.

McKeown, D. A., Muller, I.S., Gan, H., Feng, Z., Viraugh, C, .and Pegg, I. L. (2011) Vanadium and chromium redox behavior in borosilicate nuclear waste glass. Journal of Non-Crystalline Solids, 357, 2735-2743.

Miletich, R., Allan, D.R., and Angel, R.J. (1997) The synthetic Cr^{2+} silicates $BaCrSi_4O_{10}$ and $SrCrSi_4O_{10}$: The missing links in the gillespite-type $ABSi_4O_{10}$ series. American Mineralogist, 82, 697--707.

Newville, M. (2001) IFEFFIT: interactive EXAFS analysis and FEFF fitting" Journal of Synchrotron Radiation, 8, 322-324.

Novak, G.A. and Gibbs, G.V. (1971) The crystal chemistry of the silicate garnets. American Mineralogist, 56, 791-825.

Okada, A. and Keil, K. (1982) Caswellsilverite $NaCrS_2$: a new mineral in the Norton County enstatite achondrite. American Mineralogist, 67, 132-136.

Quareni, S. and De Pieri, R. (1965) A three-dimensional refinement of the structure of crocoite, $PbCrO_4$. Acta Crystallographica, 19, 287-289.

Raccah, P.M., Bouchard, R.J., Wold, A. (1966) Journal of Applied Physics, 37, 1436-1437.

Ravel, B. and Newville, M. (2005) ATHENA. ARTEMIS, HEPHAESTUS: data analysis for X-ray absorption spectroscopy using IFEFFIT. Journal of Synchrotron Radiation, 12, 537-541.

Schreiber, H. D. and Hockman, A.L. (1987) Redox Chemistry in Candidate Glasses for Nuclear Waste Immobilization. Journal of the American Ceramics Society, 70, 591–594.

Sayers, D.E. and Bunker, B.A. in: X-ray Absorption Principles, Applications, Techniques of EXAFS, SEXAFS, and XANES, ed. D.C. Kroningsberger, R. Prins (Wiley, New York, 1988), Ch. 6, p. 211.

Sutton, S.R., Jones, K.W., Gordon, B., Rivers, M.L., Bajt, S., and Smith, J.V (1993) Reduced chromium in olivine grains from lunar basalt 15555: X-ray absorption near-edge structure", Geochimica et Cosmochimica Acta, 57, 461-468.

Sutton, S.R., Bajt, S., and Jones, R. (1996) In Situ Determination of chromium oxidation state in olivine from chondrules. Lunar and Planetary Science Conference XXVII, 1291-1292.

Weisberg, M.K., Prinz, M., and Fogel, R.A. (1994) The evolution of enstatite and chondrules in unequilibtared enstatite chondrites: Evidence from iron-rich pyroxene. Meteoritics, 29, 362-373.

Weisberg, M.K., Boesenberg, J.S., Prinz, M., Clayton, R.N., and Mayeda T.K. (1995) EH3 and EL3 chondrites: a petrologic-oxygen isotope study. Lunar and Planetary Science Conference XXVI, 1481-1482.

Weisberg, M.K., Kimuar, M., McCoy, T.J., and Lin Y. (2005) Olivine and the thermal history of the E chondrite parent body", Lunar and Planetary Science Conference XXXVI, Abstract No. 1420.

Weisberg, M.K., McCoy, T.J., and Krot, A.N. (2006) Systematics and evaluation of meteorite classification" in: Meteorites and the Early Solar System II, D. S. Lauretta and H. Y. McSween Jr. (eds.), University of Arizona Press, Tucson, p.19-52

Weisberg, M.K., Ebel, D.S., Connolly, H.C., Kita N.T., Ushikubo, T. (2011) Petrology and oxygen isotope compositions of chondrules in E3 chondrites. Geochimica et Cosmochimica Acta, 75, 6556-6569.

Table 1 Cr-forsterite grain composition from SEM-EDS in wt.%. 1σ uncertainty in parentheses.

Element	Point 1	Point 2	Point 3	Average	Ideal (pure forsterite)
Mg	32.61 (0.13)	32.60 (0.13)	32.54 (0.07)	32.58 (0.11)	34.55
Cr	0.19 (0.05)	0.10 (0.05)	0.10 (0.03)	0.13 (0.04)	-
Fe	0.26 (0.06)	0.18 (0.06)	0.64 (0.03)	0.36 (0.05)	-
Mn	-	-	0.09 (0.03)	-	-
Si	21.20 (0.12)	21.31 (0.12)	21.02 (0.06)	21.18 (0.10)	19.96
O	45.74 (0.15)	45.81 (0.15)	45.60 (0.08)	45.72 (0.13)	45.49
Total	100.00	100.00	100.00	99.97	100.00

Table 2 Crocoite and uvarovite standards first shell Cr-O fitting results from EXAFS using $s_0^2 = 0.70$. E_0 values are from 5,989 eV. The r-factor is a goodness of fit parameter that is a sum-of-squares measure of the fractional misfit scaled to the magnitude of the data (Newville (2001); Ravel and Newville (2005)). Uncertainties (in parentheses) calculated by IFEFFIT.

Sample	**r-factor**	**E_0** (eV)	**r** (Å)	**n** (atoms)	**σ^2** (Å^2)
Crocoite	0.045	12.34	1.66 (0.01)	3.3 (0.4)	0.0011 (0.0018)
Actual *			1.65	4.0	
Uvarovite	0.060	-0.85	1.98 (0.01)	5.8 (0.5)	0.0009 (0.0026)
Actual **			1.98	6.0	

* Quareni and De Pieri (1965)

** Novak and Gibbs (1971)

Table 3. Cr EXAFS first and second nearest-neighbor fitting results for Cr-forsterite in meteorite MAC 88136. All fits used: $s_0^2 = 0.70$ and $E_0 = -2.12$ eV. (c) indicates constrained parameter. Conventions in Table 2 are followed here.

Sample	**r-factor**	**r** (Å)	**n** (atoms)	σ^2 (Å^2)
Meteorite Cr-O	0.16	2.02 (0.01)	2.6 (0.4)	0.0037 (0.0016)
Forsterite Mg-O				
M(1)-O *		2.10	6.0	
M(2)-O *		2.13	6.0	
Meteorite Cr-Si		2.69 (0.02)	1.8 (0.4)	0.0010 (c)
Forsterite Mg-Si				
M(1)-Si *		2.69	2.0	
M(2)-Si *		2.79	1.0	

* Boström (1987)

Table 4. Comparisons of Cr valence determinations of the Cr redox glasses from most oxidized to most reduced, using Cr XANES and colorimetry (Schreiber and Hockman (1987)). Glasses contain 1 wt.% Cr. The XANES fitting (Newville (2001); Ravel and Newville (2005)) used uvarovite (Cr^{3+}) and Cr-forsterite in MAC 88136 (Cr^{2+}) as the standards; uncertainties listed in parentheses. The associated linear combination fits of the standards XANES compared with the glass spectra are presented in Fig. 6.

Glass	Cr^{3+}	Cr^{2+}	Technique
U580	0.98 (0.02)	0.02 (0.02)	Cr XANES
	1.00		colorimetry
A303	0.84 (0.02)	0.16 (0.02)	Cr XANES
	0.79	0.21	colorimetry
U582	0.56 (0.02)	0.44 (0.02)	Cr XANES
	0.58	0.42	colorimetry
A200	0.39 (0.02)	0.61 (0.02)	Cr XANES
	0.40	0.60	colorimetry

This is a preprint, the final version is subject to change, of the American Mineralogist (MSA)
Cite as Authors (Year) Title. American Mineralogist, in press.
(DOI will not work until issue is live.) DOI: http://dx.doi.org/10.2138/am.2014.4508

Figure Captions

Fig. 1. Photo-micrograph under cross polarized transmitted light of meteorite MAC88136 featuring a forsterite-enstatite chondrule. The forsterite grain measured for this study is highlighted.

Fig. 2. Cr XANES spectra for the valence standards Cr-foil (Cr^{0}, black), uvarovite (Cr^{3+}, green), and crocoite (Cr^{6+}, red), as well as Cr-forsterite within MAC 88126 (blue).

Fig. 3a and b. $k^2\chi(k)$ (a) and partial RDF (b) data for the $Cr^{3+}O_6$ octahedral standard, uvarovite, and the Cr-forsterite grain in MAC 88136. For uvarovite, some pair correlations from the crystal structure are indicated in the partial RDF plot (green).

Fig. 4. Cr-forsterite Cr EXAFS partial RDF (top) and $k^2\chi(k)$ (bottom): data (black points and line) and fit (red line) for using a four path model. Important pair correlations are indicated.

Fig. 5. Cr-O distance (*r*) versus coordination number (*n*) of various Cr valences and environments in silicate and oxide crystals (smaller symbols). Forsterite M-site average Mg-O distances and coordination numbers are indicated (larger black points) to show the differences with the EXAFS findings (larger colored points) for the two Cr standards and Cr-forsterite in MAC 88136.

Fig. 6. Cr XANES spectra (black line and points) and fits (from IFEFFIT: red line) for the four redox glasses from Schreiber and Hockman (1987). The different Cr^{3+} and Cr^{2+} valence population for each glass from the XANES fitting is indicated. Spectra are arranged from the most oxidized (bottom) to the most reduced (top). XANES fitting used linear combinations of the Cr-forsterite data (Cr^{2+} standard) and the uvarovite data (Cr^{3+} standard).

Fig. 7. Schematic drawing of the forsterite crystal structure with Cr^{2+} entering one of the M(1) sites most likely resulting in disordered configurations intermediate between square-planar CrO_4 and octahedral M(1).

This is a preprint, the final version is subject to change, of the American Mineralogist (MSA)
Cite as Authors (Year) Title. American Mineralogist, in press.
(DOI will not work until issue is live.) DOI: http://dx.doi.org/10.2138/am.2014.4508

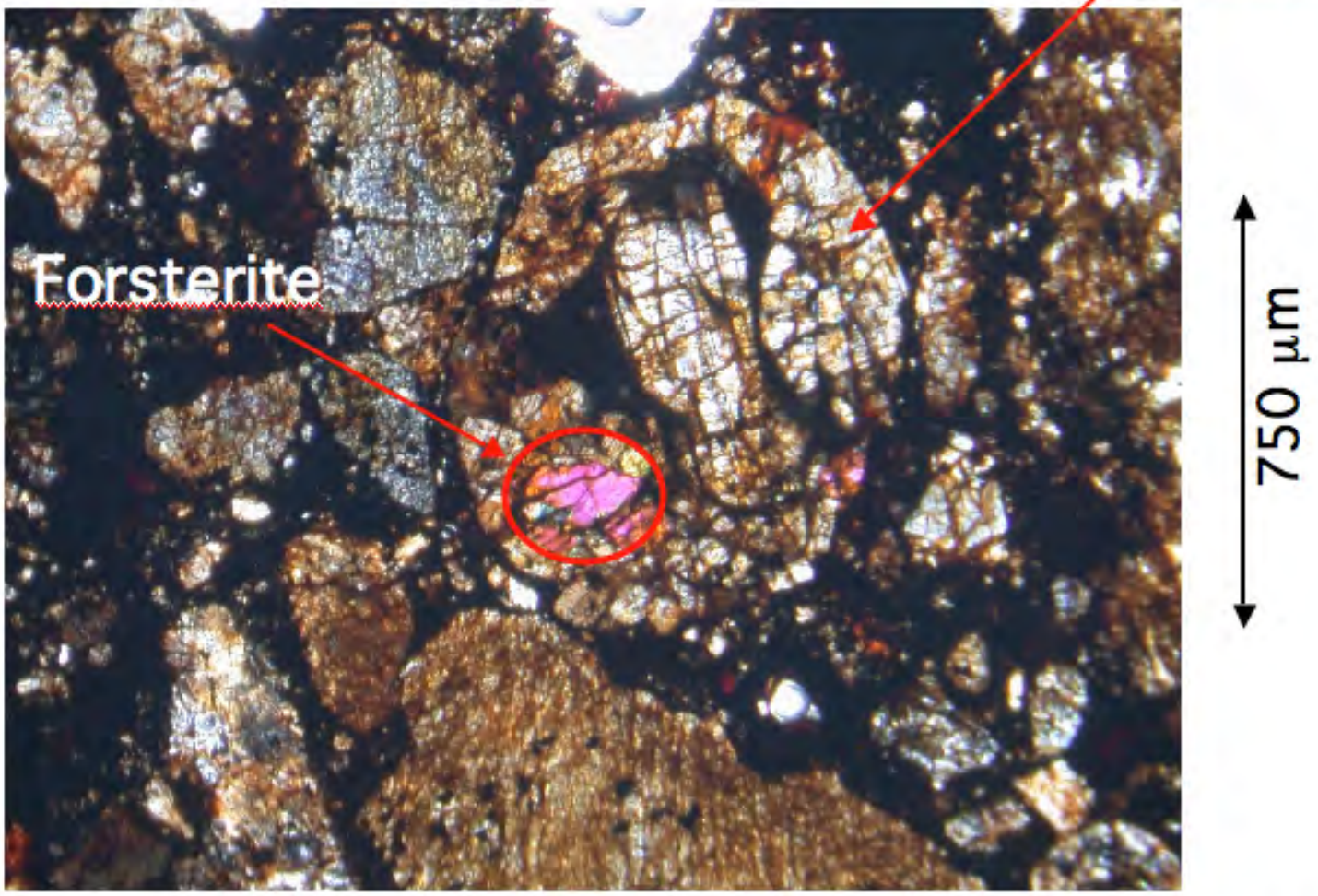

Fig. 1

This is a preprint, the final version is subject to change, of the American Mineralogist (MSA)
Cite as Authors (Year) Title. American Mineralogist, in press.
(DOI will not work until issue is live.) DOI: http://dx.doi.org/10.2138/am.2014.4508

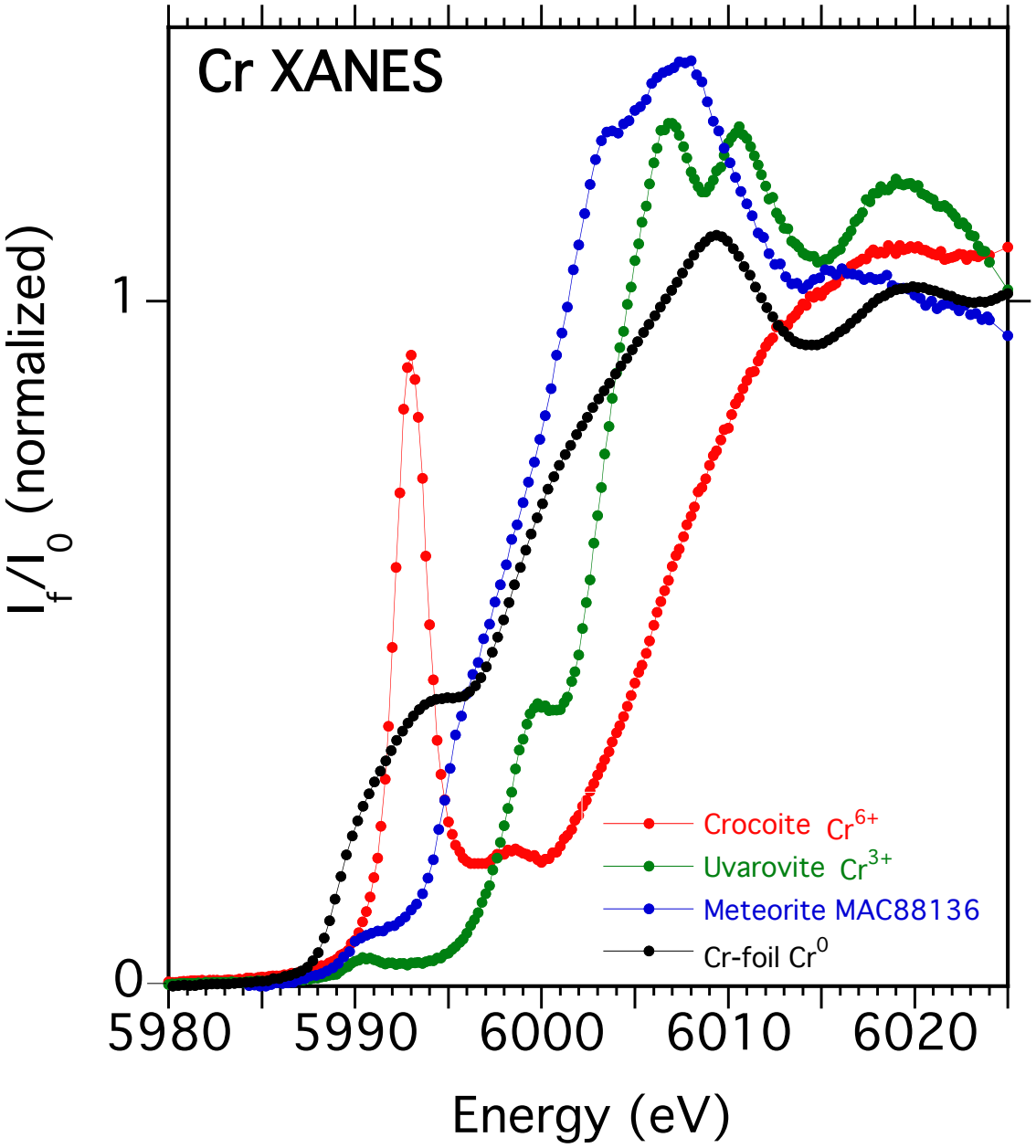

Fig. 2

This is a preprint, the final version is subject to change, of the American Mineralogist (MSA)
Cite as Authors (Year) Title. American Mineralogist, in press.
(DOI will not work until issue is live.) DOI: http://dx.doi.org/10.2138/am.2014.4508

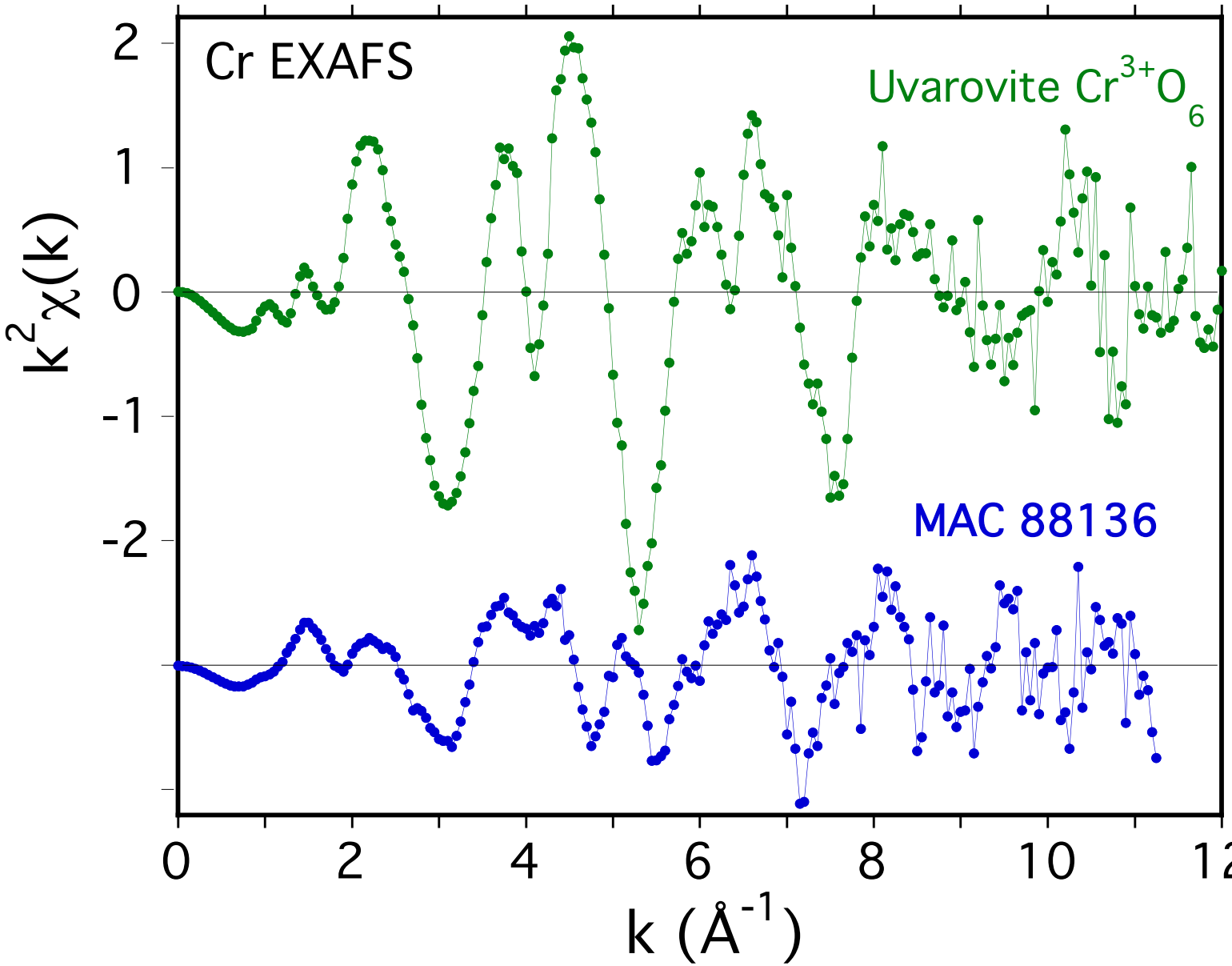

Fig. 3a

This is a preprint, the final version is subject to change, of the American Mineralogist (MSA)
Cite as Authors (Year) Title. American Mineralogist, in press.
(DOI will not work until issue is live.) DOI: http://dx.doi.org/10.2138/am.2014.4508

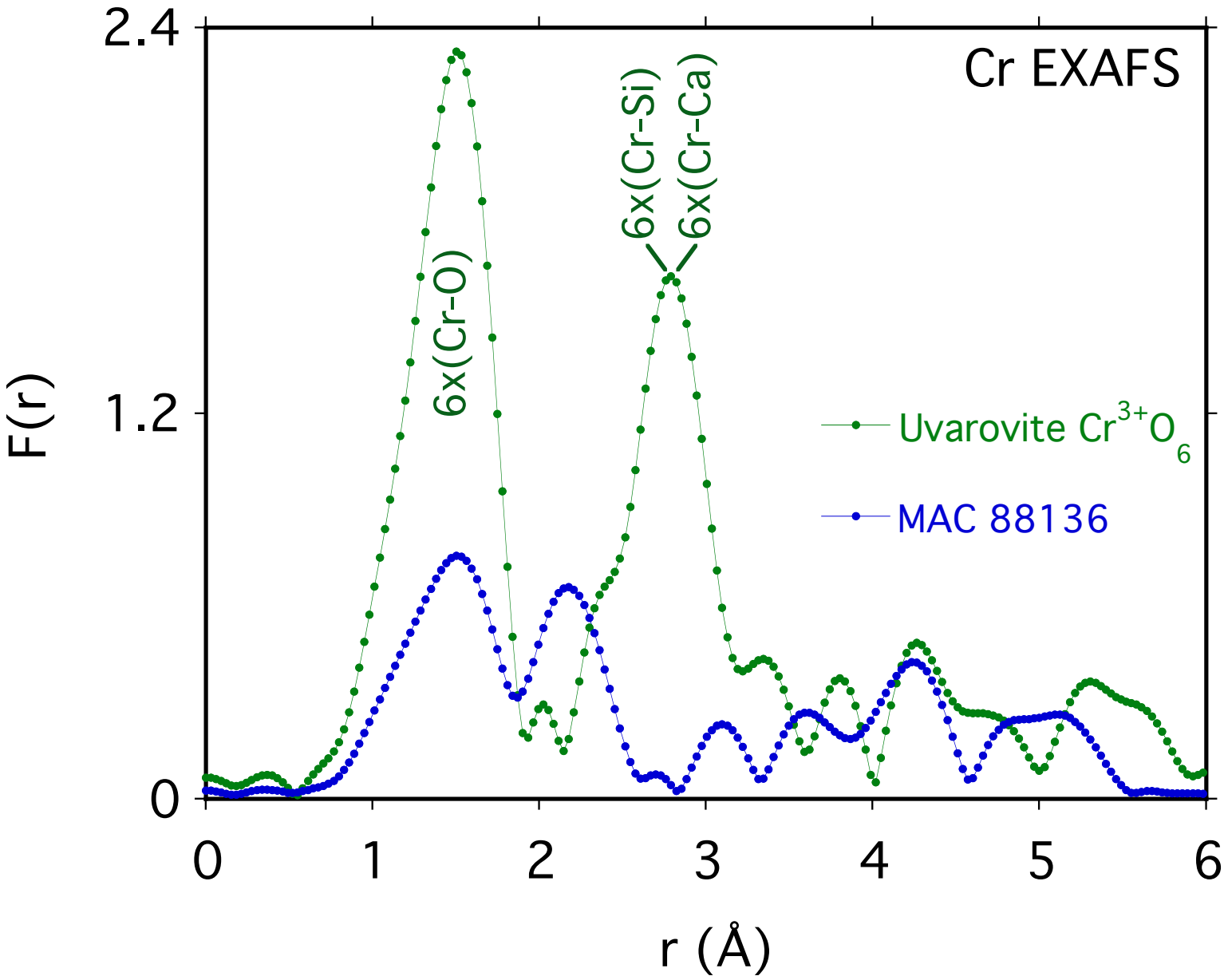

Fig. 3b

This is a preprint, the final version is subject to change, of the American Mineralogist (MSA)
Cite as Authors (Year) Title. American Mineralogist, in press.
(DOI will not work until issue is live.) DOI: http://dx.doi.org/10.2138/am.2014.4508

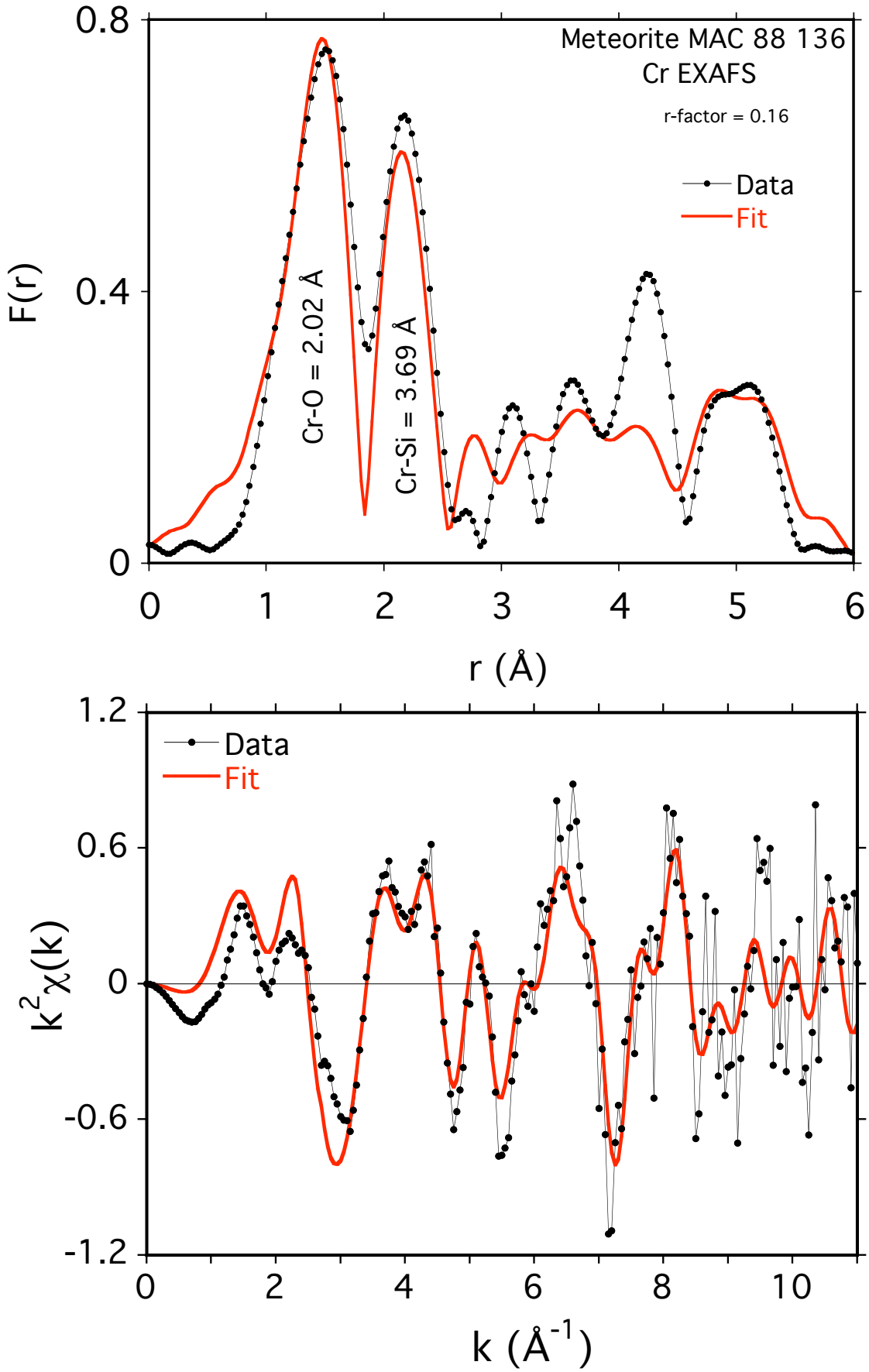

Fig. 4

This is a preprint, the final version is subject to change, of the American Mineralogist (MSA)
Cite as Authors (Year) Title. American Mineralogist, in press.
(DOI will not work until issue is live.) DOI: http://dx.doi.org/10.2138/am.2014.4508

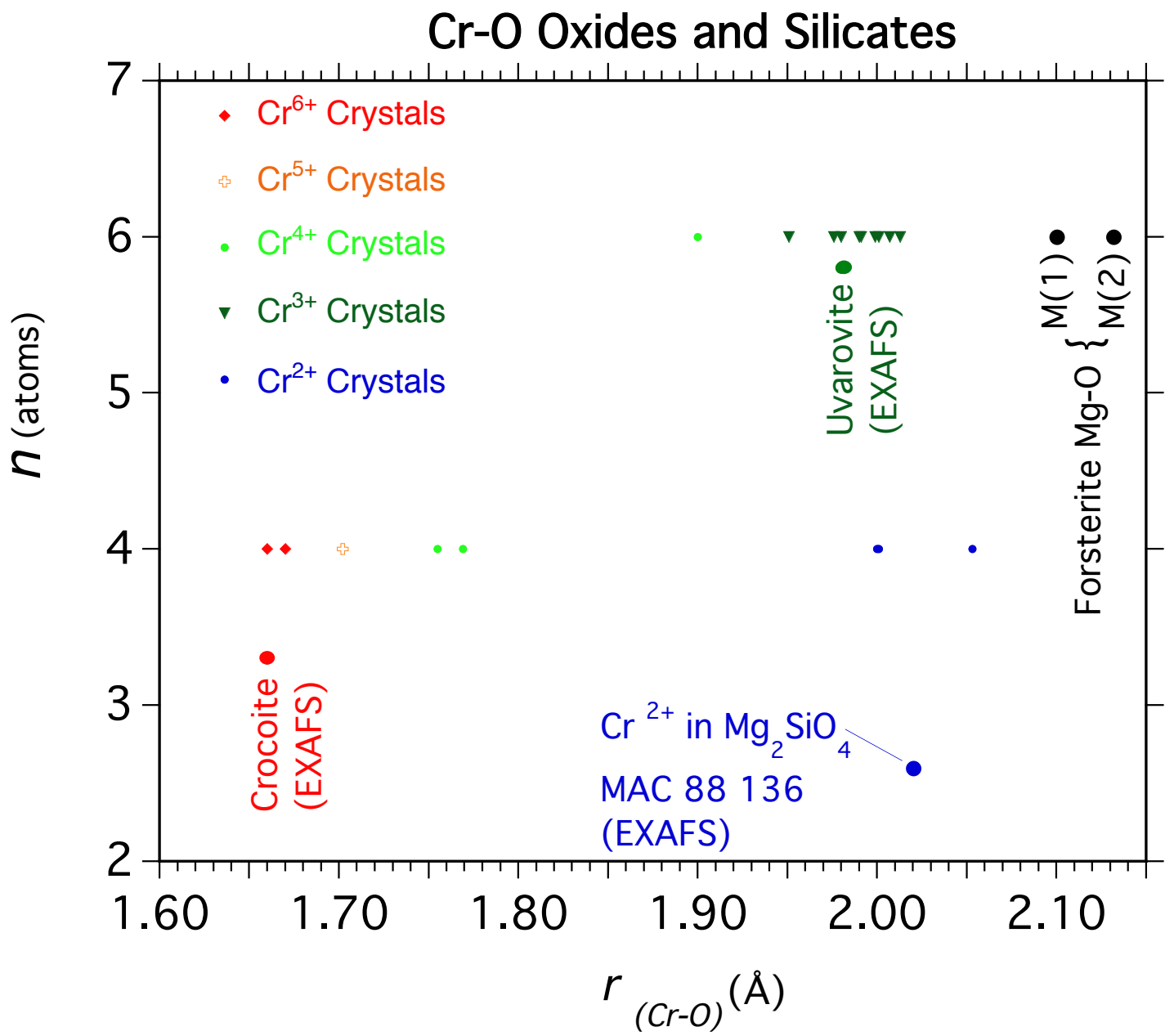

Fig. 5

This is a preprint, the final version is subject to change, of the American Mineralogist (MSA)
Cite as Authors (Year) Title. American Mineralogist, in press.
(DOI will not work until issue is live.) DOI: http://dx.doi.org/10.2138/am.2014.4508

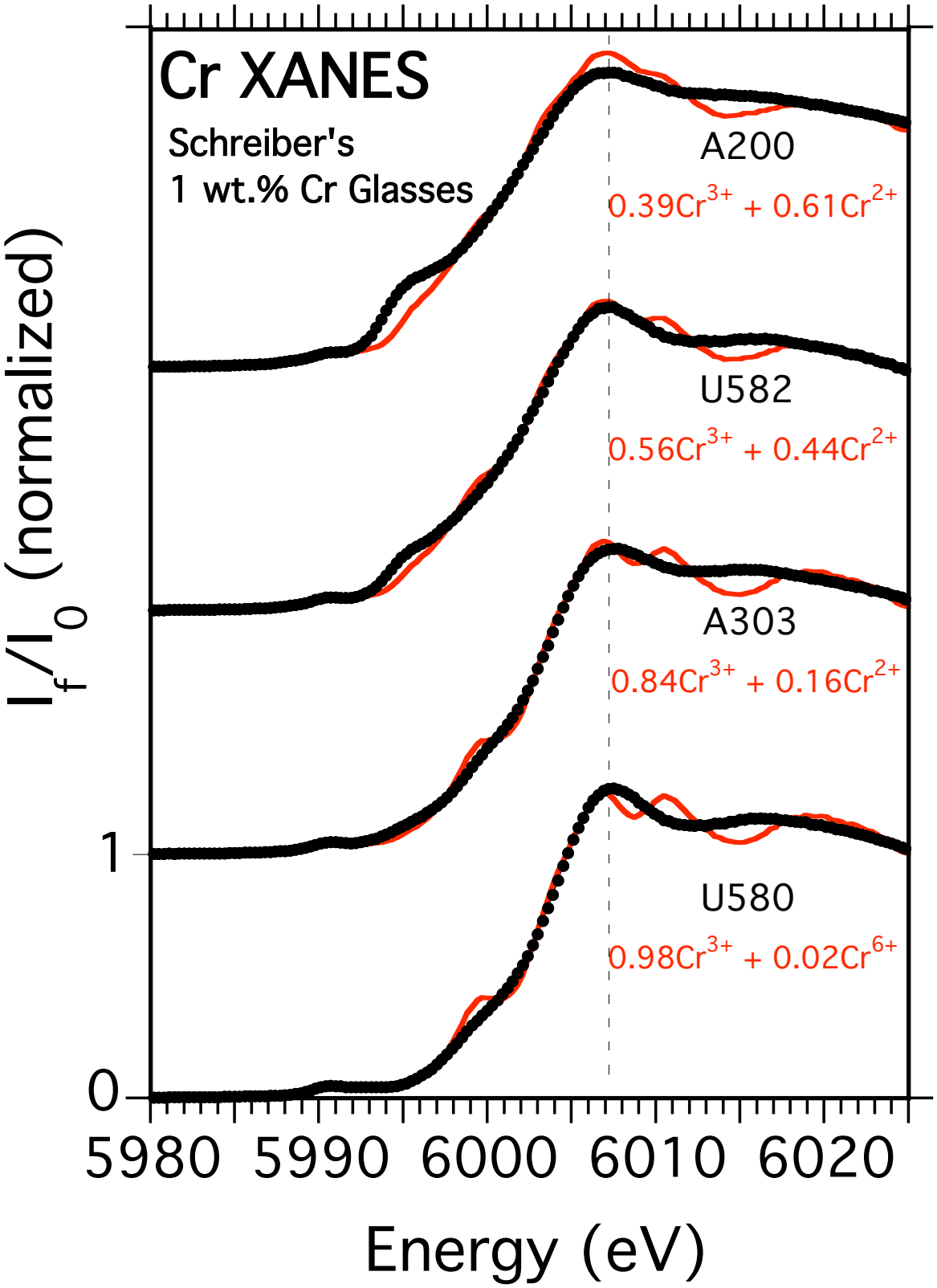

Fig. 6

This is a preprint, the final version is subject to change, of the American Mineralogist (MSA)
Cite as Authors (Year) Title. American Mineralogist, in press.
(DOI will not work until issue is live.) DOI: http://dx.doi.org/10.2138/am.2014.4508

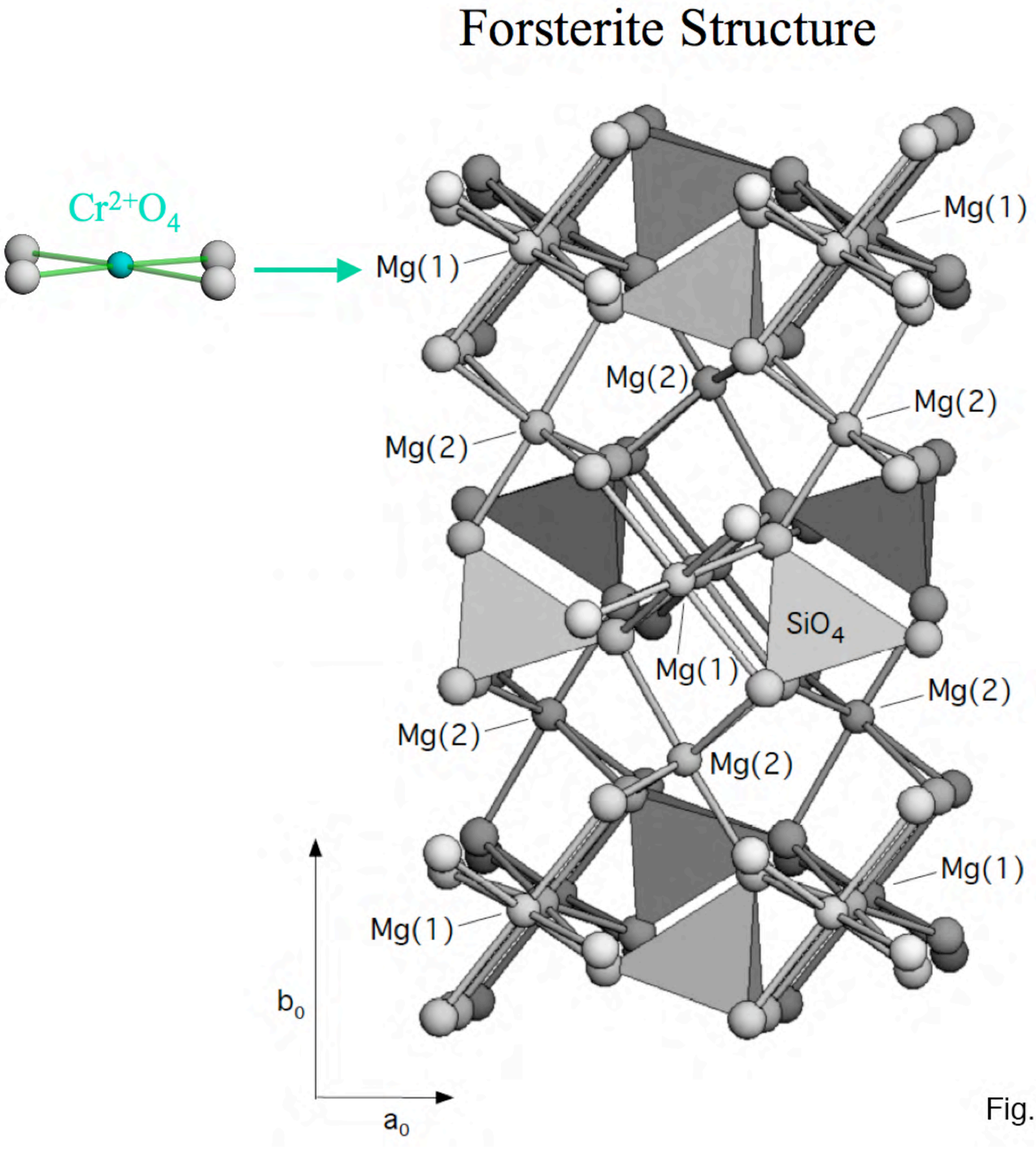

Fig. 7